

## The Crystal Structure of Livingstonite, $\text{HgSb}_4\text{S}_8$

By N. NIIZEKI<sup>1</sup> and M. J. BUERGER

With 14 figures

(Received February 25, 1957)

### Zusammenfassung

Die Raumgruppe des Livingstonits ist  $A2/a$ ; die Elementarzelle mit den Gitterkonstanten  $a = 30,25 \text{ \AA}$ ,  $b = 4,00 \text{ \AA}$ ,  $c = 21,48 \text{ \AA}$ ,  $\beta = 104^\circ 12'$  enthält 8  $\text{HgSb}_4\text{S}_8$ . Diese Formel wurde an Stelle der bisher angegebenen ( $\text{HgSb}_4\text{S}_7$ ) durch eine neue chemische Analyse gewonnen und durch die in mehreren Verfeinerungsschritten ausgeführte PATTERSON- und FOURIER-Analyse bestätigt.

Das Kristallgitter weist eine  $\text{S}_2$ -Gruppe mit einem S—S-Abstand von  $2,07 \text{ \AA}$  auf, was in Einklang mit der neuen chemischen Formel steht.

Das Gitter setzt sich aus zwei Arten von Schichten zusammen, die beide parallel (001) verlaufen. In den Schichten der einen Art werden je zwei Doppelketten von  $\text{Sb}_2\text{S}_4$  durch S—S-Bindungen in Gestalt von  $\text{S}_2$ -Gruppen, in den Schichten der zweiten Art durch Hg-Atome miteinander verknüpft. Jedes Sb-Atom hat drei S-Atome als nächste Nachbarn und weitere vier in größeren Abständen. In den Ecken eines deformierten Oktaeders um ein Hg-Atom befinden sich sechs S-Atome, von denen zwei stärker gebunden und, wie beim Zinnober  $\text{HgS}$ , linear angeordnet sind. Die vollkommene Spaltbarkeit parallel (001) kann durch das Aufbrechen der schwachen Bindungen zwischen den Schichten der beiden Arten erklärt werden.

### Abstract

The crystal structure of livingstonite has been determined. A new chemical analysis of the mineral gives the formula  $\text{HgSb}_4\text{S}_8$  instead of the previously assigned  $\text{HgSb}_4\text{S}_7$ . The space group is  $A2/a$ , and the unit-cell dimensions are  $a = 30.25 \text{ \AA}$ ,  $b = 4.00 \text{ \AA}$ ,  $c = 21.48 \text{ \AA}$ , and  $\beta = 104^\circ 12'$ . This unit cell contains 8  $\text{HgSb}_4\text{S}_8$ . Intensities were measured by the single-crystal GEIGER-counter method with  $\text{CuK}\alpha$  and  $\text{MoK}\alpha$  radiations. The structure was analyzed by direct interpretations of the PATTERSON map  $P(xz)$ , and the three-dimensional PATTERSON sections,  $P(x, n/60, z)$ . The refinement of the structure was performed by successive FOURIER and difference-FOURIER trials, and finally by the three-dimensional least-squares method. The structure obtained confirms the new chemical formula. In the structure an  $\text{S}_2$  group is found with an S—S distance of

<sup>1</sup> Present address: Mineralogical Institute, University of Tokyo, Tokyo, Japan.

2.07 Å. The existence of this  $S_2$  group was suspected from the new chemical formula. In the structure, there are two kinds of layers, both running parallel to (001). In one kind of layer, two  $Sb_2S_4$  double chains are joined together by an S—S bond to form an  $S_2$  group between them. In the other, two  $Sb_2S_4$  double chains are cemented together by Hg atoms. Each Sb atom has three closest neighboring S atoms, and four additional ones at greater distances. The coordination of the Hg atom is a distorted octahedron of six S atoms, of which two are strongly bonded ones arranged in a linear way as found in cinnabar, HgS. The perfect (001) cleavage can be explained as the breaking of the weaker bonds between the two kinds of layers.

### Introduction

There have been two crystallographic investigations of the mineral livingstonite. RICHMOND<sup>2</sup> described it as monoclinic, and GORMAN's presentation<sup>3</sup> was triclinic. BUERGER and NIIZEKI<sup>4</sup> carried out a preliminary structure determination of the mineral assuming GORMAN's triclinic cell was correct. They succeeded in obtaining the structure projected along the shortest axis (4 Å). Our result suggested doubt concerning the number of sulfur atoms in the chemical formula.

Livingstonite crystallizes in an elongated needle form with one perfect prismatic cleavage. The mineral belongs to the group of acicular sulfosalts. Structure determinations for several minerals of this group have recently been published<sup>5-9</sup>. Livingstonite is the only known sulfosalt mineral containing mercury.

### Preliminary structure investigation

For the preliminary phase of the structure investigation we are greatly indebted to Dr. GORMAN of the University of Toronto, Canada.

<sup>2</sup> W. E. RICHMOND, Crystallography of livingstonite. *Amer. Mineralogist* **21** (1936) 719.

<sup>3</sup> D. H. GORMAN, An x-ray study of the mineral livingstonite. *Amer. Mineralogist* **36** (1954) 480-483.

<sup>4</sup> M. J. BUERGER and N. NIIZEKI, The crystal structure of livingstonite,  $HgSb_4S_8$ . *Amer. Mineralogist* **39** (1954) 319-320.

<sup>5</sup> M. J. BUERGER and T. HAHN, The crystal structure of berthierite,  $FeSb_2S_4$ . *Amer. Mineralogist* **40** (1955) 226-238.

<sup>6</sup> F. E. WICKMAN, The crystal structure of galenobismutite,  $PbBi_2S_4$ . *Arkiv Min. Geol.* **1** (1951) 219-225.

<sup>7</sup> F. E. WICKMAN, The crystal structure of aikinite,  $CuPbBiS_3$ . *Arkiv Min. Geol.* **1** (1953) 501-507.

<sup>8</sup> N. NIIZEKI and M. J. BUERGER, The crystal structure of jamesonite,  $FePb_4Sb_6S_{14}$ . *Z. Kristallogr.* **109** (1957) 161-183.

<sup>9</sup> N. NIIZEKI, The crystal chemistry of the mineral sulfosalts. To appear in *Geochemica Acta*.

We were kindly offered not only a massive aggregate of cleavage flakes of livingstonite from Guerrido, Mexico, but also his original single crystal used for the above-mentioned description of his triclinic unit cell.

The first intensity data were collected from the equator WEISSENBERG photograph taken with  $\text{CuK}\alpha$  radiation<sup>10</sup>. The intensities were then

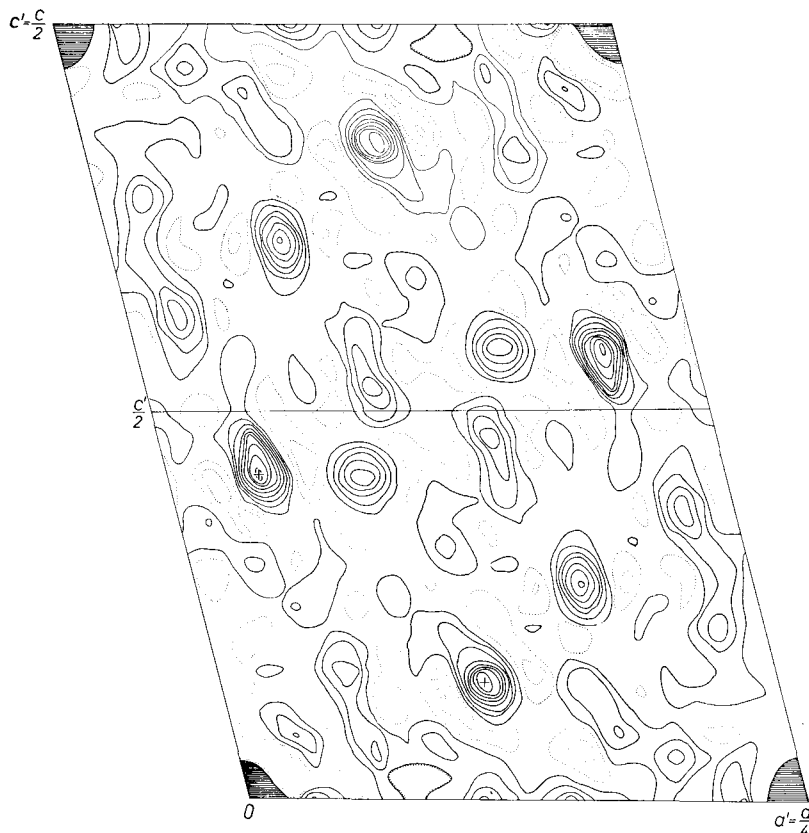


Fig. 1. PATTERSON diagram  $P(xz)$ . The dotted contours represent depressions. The details of the heavy peak at the origin are omitted.

corrected for LORENTZ and polarization factors, but no allowance was made for absorption. The resulting  $F^2(h0l)$ 's were used to prepare the PATTERSON map,  $P(xz)$ , Fig. 1.

Since GORMAN's unit cell contained  $\text{HgSb}_4\text{S}_7$ , there is only one Hg atom in the cell. Its position is fixed at a center of symmetry if the

<sup>10</sup> RALPH H. V. M. DAWTON, The integration of large numbers of x-ray reflections. Proc. Phys. Soc. [London] 50 (1938) 919-925.

space group is  $P\bar{1}$ . A statistical check of the centrosymmetry<sup>11</sup> was applied to the observed intensity data, and the resulting curve is shown in Fig. 2. Although the chemical composition of the mineral is not ideal for the statistical treatment, the result was considered as indicating a center of symmetry in the projection.

Once the position of the mercury atom was fixed, the interpretation of the PATTERSON map, Fig. 1, was straightforward. The two heavy

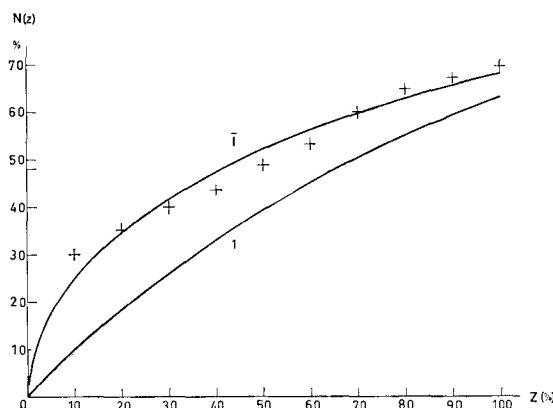


Fig. 2. Statistical test of the centrosymmetry. The theoretical curve for the centrosymmetric crystal is designated by  $\bar{I}$ , and for the noncentrosymmetric crystal by 1. The crosses represent the result with  $F^2(h0l)$ 's of livingstonite.

peaks, indicated by crosses in Fig. 1, must be due to Hg—Sb interactions. Since Hg is at the origin, these peaks could be assumed as the atomic sites for the two Sb atoms in the asymmetric unit. The first FOURIER map of the projection, Fig. 3, was computed using signs determined by heavy atoms only, provided the contributions to the amplitudes by them exceeded one third of the observed values. From this map information concerning the locations of the S atoms could be obtained. The structure was refined by four successive FOURIER trials. With an assumed chemical formula of  $\text{HgSb}_4\text{S}_7$ , one of the S atoms must be placed on one set of centers of symmetry. From these FOURIER trials, however, the following facts became evident: First, there are two peaks surrounding the center of symmetry at  $(\frac{1}{2} 0 \frac{1}{2})$  each with peak heights as high as the other three kinds of S atoms. Second, there is no indication of an atom on the center of symmetry, and the sign changes caused

<sup>11</sup> E. R. HOWELLS, D. C. PHILLIPS and D. ROGERS, Experimental investigation and the x-ray detection of centers of symmetry. *Acta Crystallogr.* **3** (1950) 210—214.

by placing one S atom on this inversion center did not bring back the assumed atom onto the center in the resulting FOURIER map. The atomic coordinates of the fourth trial are tabulated in Column I of Table 1.

If the peak at  $x = 0.598$ ,  $z = 0.444$  did actually represent the fourth S atom in the asymmetric unit, the chemical formula of livingstonite should be  $\text{HgSb}_4\text{S}_8$  instead of  $\text{HgSb}_4\text{S}_7$ .

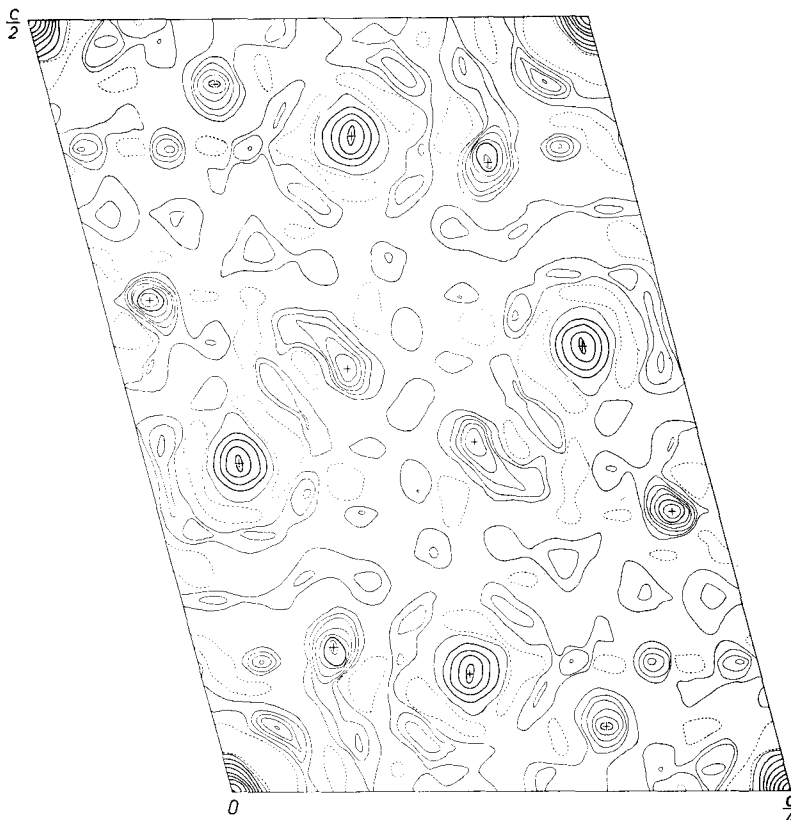


Fig. 3. The first electron-density map  $\rho(xz)$ . The broken lines represent depressions. One interval between heavy contours corresponds to five intervals of light contours. The details between successive heavy contours are omitted. The crosses indicate the atomic sites listed in Column I of Table 1.

#### Chemical composition of livingstonite

In the face of this anomaly of composition, it was felt that new data for the chemical composition of the mineral, as well as more exact X-ray diffraction data, were essential. A specimen from Huitzco, Mexico, was kindly offered for this purpose by Dr. FOSHAG of the

National Museum, Washington, D.C. This specimen (U.S. National Museum No. 105 163) was a beautiful crystal of selenite with numerous inclusions of fine needles of livingstonite.

First the selenite crystal was carefully cleaved to separate the livingstonite needles. After repeated washings in a warm dilute solution of hydrochloric acid, the remaining grains of selenite were separated by the heavy liquid method. Finally the sample was placed under the binocular for manual separation of the mineral. The material collected

Table 1. *Coordinates of atoms referred to projected cell with  $a' = \frac{a}{4}$  and  $c' = \frac{c}{4}$*

Atom		I DAWTON data	II GEIGER- counter data
Hg	$x'$	.000	.000
	$z'$	.000	.000
Sb <sub>I</sub>	$x'$	.479	.482
	$z'$	.150	.153
Sb <sub>II</sub>	$x'$	.170	.170
	$z'$	.429	.423
S <sub>I</sub>	$x'$	.243	.237
	$z'$	.160	.185
S <sub>II</sub>	$x'$	.915	.910
	$z'$	.364	.363
S <sub>III</sub>	$x'$	.693	.685
	$z'$	.085	.081
S <sub>IV</sub>	$x'$	.598	.597
	$z'$	.444	.443

Table 2. *Analysis of livingstonite*

Element	Weight percent	
Hg	19.49 %	
Sb	50.46	
S	27.61	
As	0.29	
Fe	0.22	
Pb	0.24	
Si	0.1–1.0 %	} estimated by spectro- graph
Al	0.1–1.0 %	
Ca	500–3000 ppm.	
Cu	200–1000 „	
Mg	100–500 „	
Bi	100–500 „	
Mn	50–300 „	
Ag	5–25 „	
Na	5–25 „	
Tl	2–10 „	

was then chemically and spectrographically analyzed. The result of this analysis is tabulated in Table 2.

The interpretation of the chemical data was carried out under the following two assumptions. First, Si and Al detected by the spectrograph were presumed due to minor impurities of some kind of unidentified silicate mineral which escaped separation. Later it was observed that some livingstonite needles were aggregated around impurity grains as cores. Second, As was assumed to substitute for Sb, and it was assumed that Pb and Fe could occupy Hg sites.

The weight percentages of Al and Si were subtracted from the total amount. The amount subtracted was half of the value of the maximum estimation by the spectrographical method. The values determined in

this way (1.1 % for Si, and 0.6 % for Al) summed to 1.7 %, which was very close to the deficiency of the total weight percentage of the major elements from 100 %. The elements Hg, Pb, and Fe were grouped together in one group, and Sb and As into another group, as shown in Column I of Table 3. All the other minor elements were neglected. Then these three values for (Hg, Pb, Fe), (Sb, As) and S were converted into the values listed in Column II of Table 3 to make up the total to 100 %.

Table 3. *Interpretation of chemical data*

Element	I Original Analysis	II Normalized to 100 %	III $\text{HgSb}_4\text{S}_7$	IV $\text{HgSb}_4\text{S}_8$
	%	%	%	%
Hg	19.49	20.29	21.99	21.25
Pb	0.24			
Fe	0.22			
Sb	50.46	51.63	53.40	51.48
As	0.29			
S	27.61	28.08	24.61	27.17
Total	98.31	100.00	100.00	100.00
Density measured	5.00 (FRONDEL)			
Density computed			4.88	5.06

In Columns III and IV of Table 3, the ideal weight percentages of the composition  $\text{HgSb}_4\text{S}_7$  and  $\text{HgSb}_4\text{S}_8$  are tabulated. Comparison of the result in the Column II with these two kinds of ideal composition indicated definitely the composition  $\text{HgSb}_4\text{S}_8$  as that of livingstonite. The value of the density, 5.00, measured by FRONDEL<sup>12</sup>, was found to agree well with 5.06, the calculated density of  $\text{HgSb}_4\text{S}_8$ .

#### Unit cell dimensions and space group

Several good single crystals were selected for the X-ray investigation from the livingstonite needles used for the chemical analysis. WEISSENBERG, precession, and DE JONG photographs were taken for the equator and up to the 4th layer, with the crystal set so that the needle axis was parallel to the goniometer axis. The crystals used for the preliminary stage were re-examined by the same methods, and were identified as the same material as the needles.

<sup>12</sup> C. PALACHE, H. BERMAN and C. FRONDEL, *The System of Mineralogy* (John Wiley and Sons, New York: 1952) 485–486.

The crystal was monoclinic, and the unit-cell dimensions obtained were as follows:

$$\begin{aligned} a &= 30.25 \text{ \AA} \\ b &= 4.00 \text{ \AA} \quad \beta = 104^\circ 12'. \\ c &= 21.48 \text{ \AA} \end{aligned}$$

This unit cell contains  $8\text{HgSb}_4\text{S}_8$ .

The following systematic absences were observed for the recorded spectra:

$$\begin{aligned} hkl &\text{ with } k + l = \text{even only} \\ h0l &\text{ with } l = \text{even, and } h = 4n \text{ (} n = 0, 1, 2, 3, \dots \text{) only.} \\ 0k0 &\text{ with } k = \text{even only} \end{aligned}$$

From these rules the space group is  $A2/a$  if it is centrosymmetric, and  $Aa$  if non-centrosymmetric. The observed systematic absences for reflections  $h0l$  are rather unusual. For the two possible space groups the required systematic absences for this type of reflection are  $h = \text{odd}$  and  $l = \text{odd}$ . Therefore, the extra systematic absences with  $h = 4n + 2$ , and  $l = \text{odd}$  are to be interpreted as due to the structural arrangement. Satisfactory twinning rules to explain the above-mentioned facts could not be obtained. The centrosymmetrical space group  $A2/a$  was assumed for the starting point.

#### Relations between unit cell data

Because of the extinction already described, a sub-multiple cell with  $a' = a/4$ , and  $c' = c/2$  could be taken for the projection on (010). These dimensions are as follows:

$$\begin{aligned} a' &= 7.56 \text{ \AA} \\ c' &= 10.74 \text{ \AA} \quad \beta = 104^\circ 12'. \end{aligned}$$

These values were identical with those obtained at this stage by checking GORMAN's result from the equator WEISSENBERG photograph. There must be some relation between the present unit cell and the ones previously described by RICHMOND and GORMAN. The relations between these unit cells are tabulated in Table 4.

Our cell and RICHMOND's are almost identical except that our  $a$  unit is double RICHMOND's. GORMAN's triclinic cell can be explained as a primitive triclinic setting of our  $A$ -centered monoclinic cell if taken with the sub-multiple units,  $a' = a/4$ , and  $c' = c/2$ . The three shortest vectors of this setting of our cell are represented by vectors  $A$ ,  $B$ ,



and  $C$  in Table 4. The vectorial expression of these three new axes is also found in Table 4. The good agreement between this cell and GORMAN's cell supports the relation discussed above.

Space group  $A2/a$  is illustrated in Fig. 4 by projections along the  $b$  and  $c$  axes. The sub-multiple unit cell in the projections on  $(010)$  is indicated by a heavy outline in the drawing. The statistical test with

Table 4. Comparison of cell data for livingstonite

	RICHMOND	GORMAN (original kX units converted to Å units)	NIIZEKI and BUERGER	NIIZEKI and BUERGER's cell referred to $A = \frac{1}{4}a - \frac{1}{2}b$ $B = \frac{1}{2}b - \frac{1}{2}c$ $C = b$
$a$	$15.14 \text{ \AA} = 7.57 \cdot 2$	$7.67 \text{ \AA}$	$30.25 \text{ \AA} = 7.64 \cdot 4$	$7.62 \text{ \AA}$
$b$	3.98	4.00	4.00	4.00
$c$	$21.60 = 10.80 \cdot 2$	10.84	$21.49 = 10.75 \cdot 2$	10.93
$\alpha$	—	$99^\circ 12'$	—	$100^\circ 31'$
$\beta$	$104^\circ 00'$	$102^\circ 01'$	$104^\circ 12'$	$104^\circ 49'$
$\gamma$	—	$73^\circ 48'$	—	$73^\circ 46'$
cell contents	$4 \text{ HgSb}_4\text{S}_7$	$\text{HgSb}_4\text{S}_7$	$8 \text{ HgSb}_4\text{S}_8$	$\text{HgSb}_4\text{S}_8$

$F^2(h0l)$ 's, which was considered to indicate the existence of the center of symmetry in the projection, must now be interpreted as the proof of a pseudo center of symmetry at  $(\frac{1}{8}, 0, \frac{1}{4})$ , which is indicated by a cross in Fig. 4.

### Three-dimensional intensity determination

Three-dimensional intensities were collected by the single-crystal GEIGER-counter-goniometer method developed in the Crystallographic Laboratory of M.I.T. The  $h0l$  intensities were first measured with  $\text{MoK}\alpha$  radiation. But the large size of the true unit-cell dimensions made the successive reciprocal-lattice points in the upper levels too close to be resolved by this radiation. Thus  $\text{CuK}\alpha$  radiation was necessary for collecting the  $hkl$  intensities, although this longer wavelength resulted in an increase in the linear absorption coefficient of the crystal. These intensities were corrected for LORENTZ and polarization factors, but no allowance was made for absorption factor until the last stage of analysis.

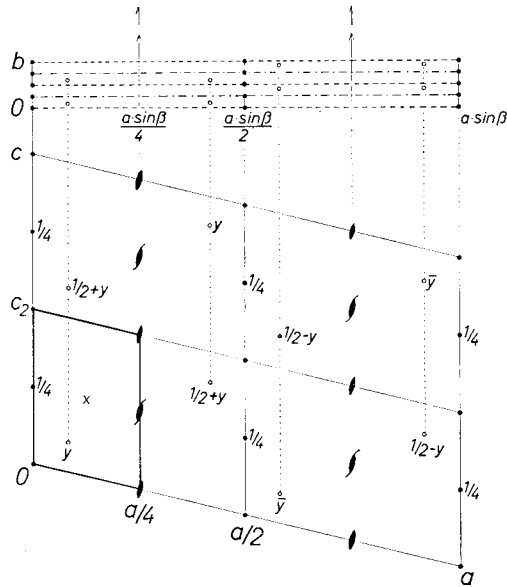


Fig. 4. Representations of space group  $A2/a$ . The lower drawing shows the symmetry elements and the general equipoint  $8(f)$  in the projection on  $(010)$ . The heavy outline in this diagram indicates the sub-multiple unit cell of the projection. A cross inside this unit shows the location of the pseudo center of symmetry. The upper drawing represents the projection on the plane normal to the  $c$  axis.

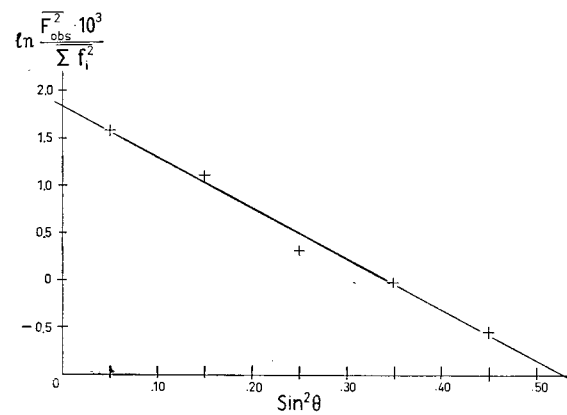


Fig. 5. Determination of scale factor and temperature coefficient of livingstonite by WILSON's statistical method. The observed  $F^2(h0l)$ 's collected with  $\text{MoK}\alpha$  radiation were used to obtain the result.

### Refinement of the projected structure

With the new set of  $F^2(h0l)$ 's collected with  $\text{MoK}\alpha$  radiation, the refinement of the electron-density map  $\rho(xz)$  was carried out. The statistical treatment of WILSON<sup>13</sup> applied to the  $F^2$  values, shown in Fig. 5, determined the scaling factor and temperature coefficient. With

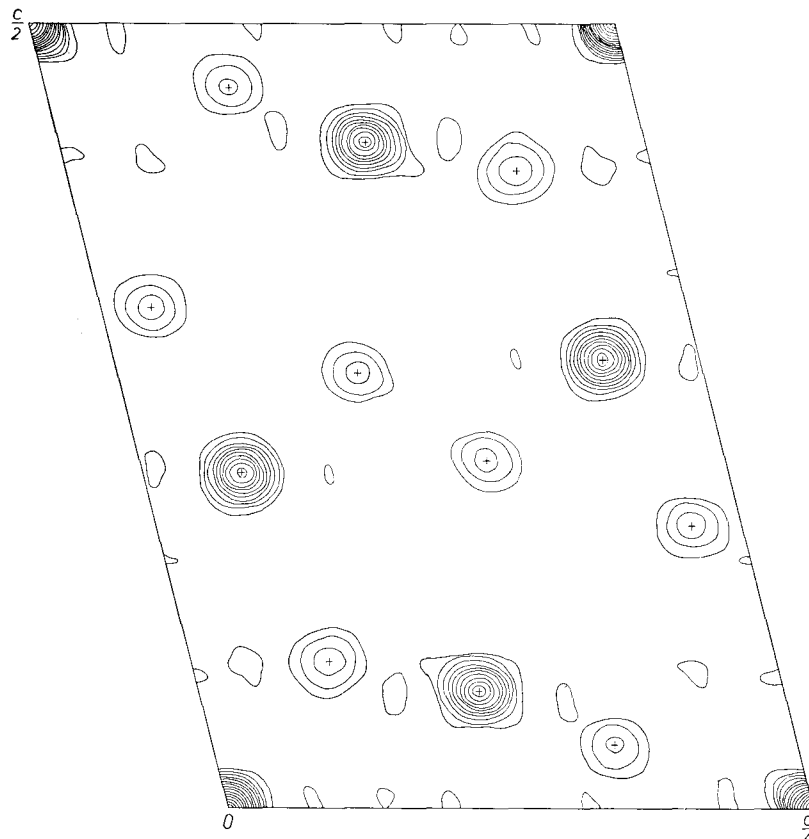


Fig. 6. Final electron-density map of the projection on (010). This  $\rho(xz)$  map represents the crystal structure in the sub-multiple unit cell outlined by heavy lines in Fig. 4. Negative contours are omitted.

the final atomic coordinates determined in the preliminary stage, and these new  $F^2$  values, the refinement of the projection was done by successive FOURIER and difference-FOURIER trials. The final atomic coordinates are tabulated in Column II of Table 1. The temperature

<sup>13</sup> A. J. C. WILSON, Determination of absolute from relative x-ray intensity data. *Nature* **150** (1942) 151–152.

coefficient determined from Fig. 5 was  $B = 1.32$ . The reliability factor with the final atomic coordinates was computed as  $R = 0.133$ . The final electron-density map  $\rho(xz)$  is presented in Fig. 6. In this map it is clearly shown that the structure determination confirms the new chemical composition of livingstonite,  $\text{HgSb}_4\text{S}_8$ .

### Determination of $y$ coordinates

*Introduction.* The comparison between the projection of the structure, Fig. 6, and the structures of other acicular sulfosalts previously analyzed permitted understanding the general scheme of the structure without difficulty. All the atoms were found to be located very close to the  $a$  glide-planes at  $y = 0$ , or  $1/2$ . The deviation of the  $y$  coordinates from these values were considered too small to be detected by crystal-chemical considerations. Also the other two available projections along the longer axes were expected to give results with considerable overlappings of atoms. More exact  $y$  coordinates of the heavy atoms were determined from the direct interpretation of the three-dimensional PATTERSON sections.

*Three-dimensional PATTERSON sections.* The three-dimensional PATTERSON sections were prepared with  $F^2(hkl)$ 's collected with  $\text{CuK}\alpha$  radiation. FOURIER summations of the type

$$P\left(u, \frac{n}{60}, w\right) = \sum_h \sum_k \sum_l |F(hkl)|^2 \cos 2\pi\left(hu + k\frac{n}{60} + lw\right)$$

were computed for the values of  $n = 0, 2, 4, \dots$  and up to 14. The resulting maps comprising eight sections are shown in Fig. 10.

The space group of the crystal is  $A2/a$ . The space group of PATTERSON space corresponding to  $A2/a$  is  $A2/m$ . This space group  $A2/m$  is illustrated in Fig. 7. Because of the  $A$  centering, the section at  $y = 1/2$  is identical with that at  $y = 0$  combined with a shift of origin of  $c/2$ . The following relation exists among the various sections:

Section  $(30 + n)/60 =$  section  $n/60$  plus shift of origin by  $c/2$ .

Also there are two mirror planes at  $y = 0$ , and  $1/2$ . Because of these mirror operations there are two further relations among sections:

$$\begin{aligned} \text{Section } n/60 &= \text{section } (-n)/60, \text{ and} \\ \text{section } (30 + n)/60 &= \text{section } (30 - n)/60. \end{aligned}$$

The above considerations show that the sections between  $0/60$  and  $15/60$  are enough to represent the whole PATTERSON space. The other sections are related to these as indicated in the following table.

Section	Section	
$16/60 = 14/60$	$45/60 = 15/60$	} without shift
$17/60 = 13/60$	$46/60 = 14/60$	
.....	.	
$29/60 = 1/60$	.	
$30/60 = 0/60$	.	
$31/60 = 1/60$	$59/60 = 1/60$	
.....		
$44/60 = 14/60$		

} plus a shift of  
origin by  $c/2$

*Interpretation of the three-dimensional PATTERSON peaks.* The unit cell contains  $8\text{HgSb}_4\text{S}_8$ . Equipoint considerations fix the locations of two kinds of Hg.  $\text{Hg}_I$  is placed at the center of symmetry  $4(b)$ .  $\text{Hg}_{II}$  is

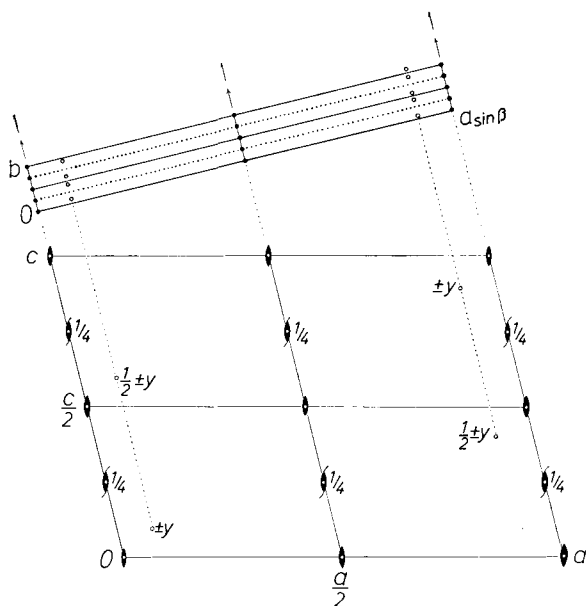


Fig. 7. Two projections of space group  $A2/m$ . The lower drawing shows the symmetry elements and the general equipoints  $8(j)$  in the projection on  $(010)$ .

The upper drawing shows the projection on the plane normal to the axis.

on the two fold axis  $4(e)$ . All the rest of the atoms occupy the general position  $8(f)$ . The  $\text{Hg}_I$ — $\text{Hg}_{II}$  PATTERSON peaks were easily identified, and it was found that between  $y_{\text{Hg}_I}$  and  $y_{\text{Hg}_{II}}$  there was a difference of  $b/2$ . There are four different kinds of Sb atoms in the unit cell. Two kinds of approach to determine the  $y$  coordinates of these Sb atoms were tried:

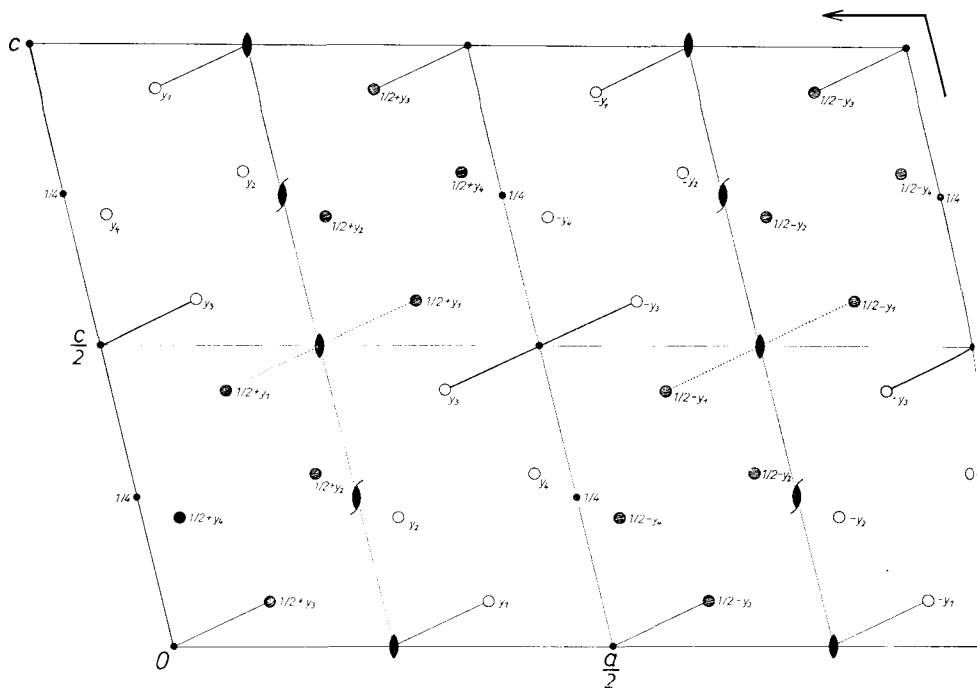


Fig. 8. Projection of the Sb atoms in the whole unit cell on (010). The open circles indicate  $y$  coordinates close to zero, and the shaded circles indicate  $y$  coordinates close to  $1/2$ .

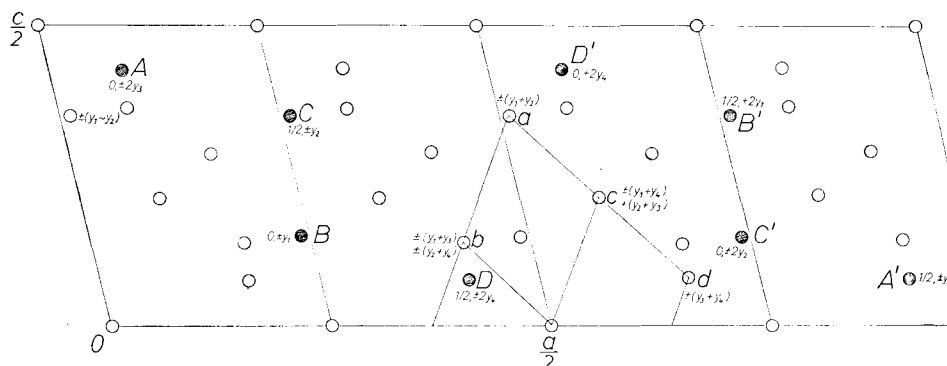
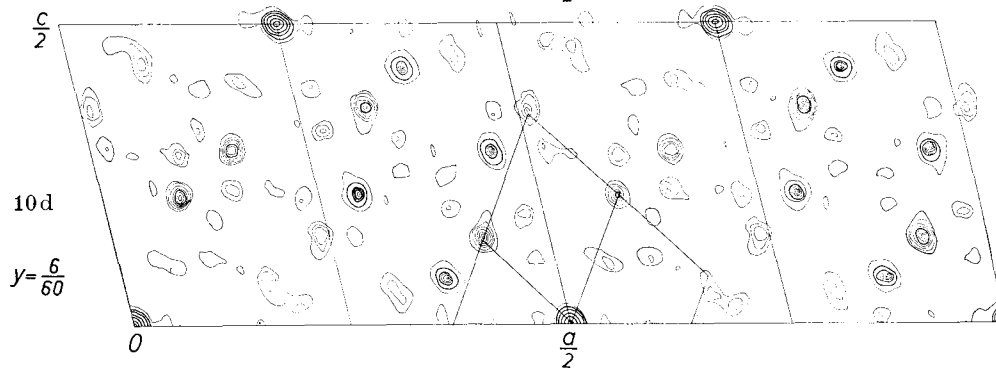
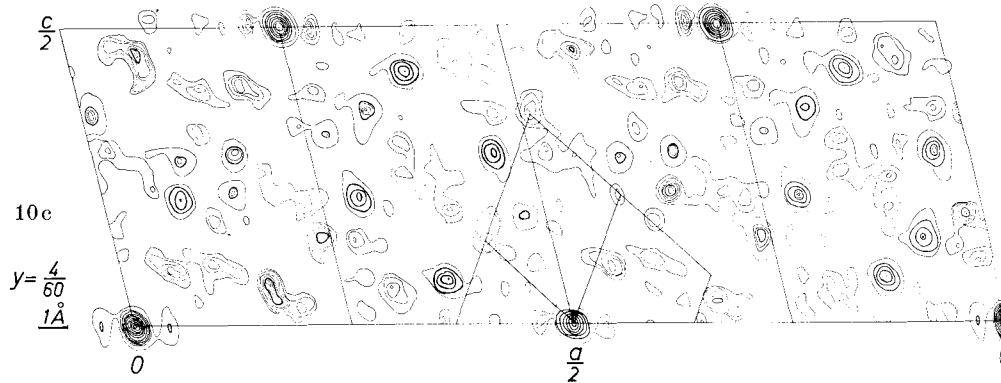
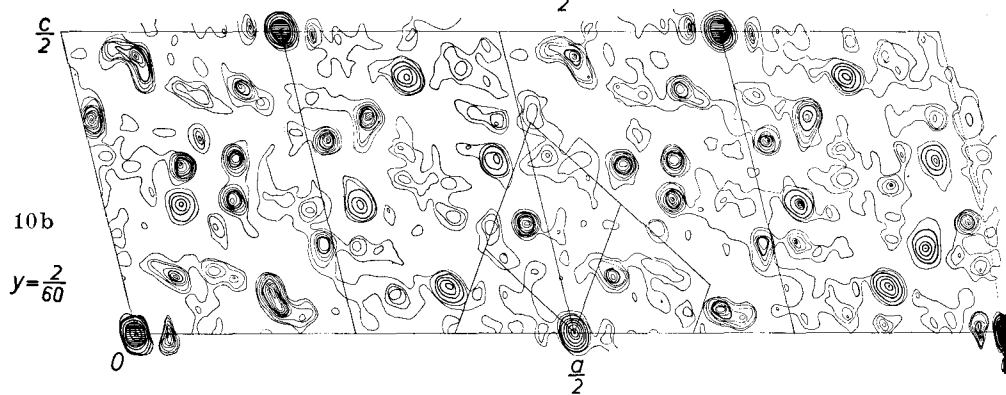
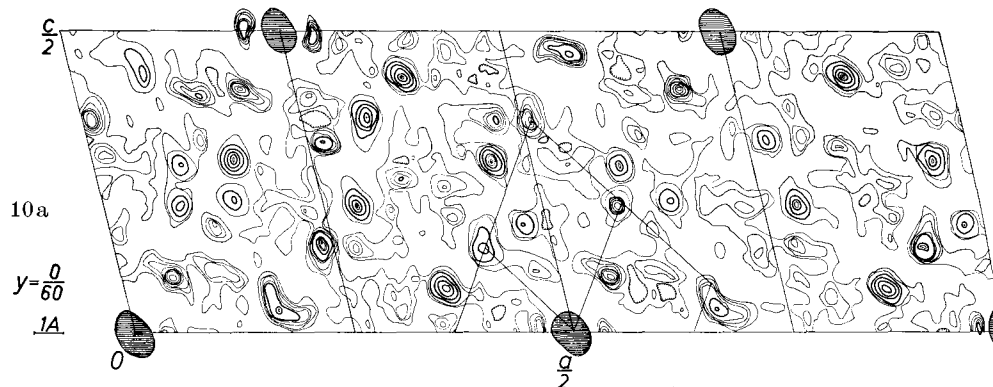


Fig. 9. The vector set constructed from the point set of the Sb atoms, Fig. 8. The positions of PATTERSON peaks are indicated by circles. Shaded circles designated by letters  $A$ ,  $B$ ,  $C$ , and  $D$  indicate the inversion peaks. The open circles with letters  $a$ ,  $b$ ,  $c$ , and  $d$  are the peaks used for the determination of  $y$  coordinates of Sb atoms. These peaks are connected by straight lines so that the identification of them in the PATTERSON sections (Fig. 10) becomes easy. Computed  $y$  coordinates of these peaks are also found in the diagram.

*Interpretation of Hg—Sb peaks.* The Hg—Sb peaks could easily be identified in the PATTERSON sections. Since one kind of Hg is located on a center of symmetry, the  $y$  coordinates of Sb can be determined if the Hg—Sb peaks are clearly defined in the sections. Unfortunately the deviations of the  $y$  coordinates from zero or  $1/2$  are small, so the maximum contour of the  $\text{Hg}_I\text{—Sb}$  peak should be located very close to section 0/60. As mentioned before there is a mirror operation at level 0/60. Thus the peak very close to section 0/60 overlaps its mirror equivalent. As the result, all the  $\text{Hg}_I\text{—Sb}$  peaks give elongated peak volumes with their maximum contours in the section 0/60. Thus the more exact determination of  $y_{\text{Sb}}$ 's from this approach was impractical.

*Interpretation of Sb—Sb peaks.* In Fig. 8, the projected locations of the Sb atoms are illustrated. Approximate  $y$  coordinates determined as 0 and  $1/2$  are indicated respectively by open and shaded circles. From this projection of the heavy atoms the vector set of the Sb atoms can be constructed, and the result is shown in Fig. 9. There are two kinds of Sb—Sb peaks. One corresponds to the interatomic vector between an Sb and its symmetrical equivalents. They are, for example,  $\text{Sb}_I\text{—Sb}_I$  inversion peaks, rotation peaks generated by a 2-fold rotation axis or a 2-fold screw axis, and glide-related peaks. The rotation peaks were not useful in determining the  $y$  coordinates; that is, the coordinates along the rotation axis. Since the glide peaks have special values for  $x$  and  $z$ , considerable overlapping results and the decomposition of the glide peak into each component is impossible. Although the consideration of the inversion peaks is most appropriate in the usual case, the situation with livingstonite makes the interpretation of the inversion peak difficult. The reason is as follows: Because of the sub-multiple unit cell observed in the projection on (010), the inversion peak of an atom and the rotation peak of an atom, related to the former atom by the pseudo center of symmetry, have identical  $x$  and  $z$  coordinates. For example, in Fig. 8, the  $\text{Sb}_{\text{III}}\text{—Sb}_{\text{III}}$  inversion vector is drawn with a heavy line, and the  $\text{Sb}_I\text{—Sb}_I$  rotation vector with a dotted line. These two vectors give their peaks at the same location indicated by the letter  $B$  in Fig. 9. The  $y$  coordinates of the peaks are  $2y_3$  and zero. It can also be seen that the  $\text{Sb}_I\text{—Sb}_I$  inversion vector, and the  $\text{Sb}_{\text{III}}\text{—Sb}_{\text{III}}$  rotation vector, indicated by light lines in Fig. 8, also give their peaks at the same location in the projection, with  $y$  coordinates of  $2y_1$  and zero. Thus if the  $y$  coordinates do not deviate much from zero, the overlapping with the rotation peak at section 0/60 obscures the definite maximum contour representing  $2y_1$  and  $2y_3$ .





The second kind of Sb—Sb peak represents interatomic vectors between different kinds of Sb atoms, such as  $\text{Sb}_\text{I}$ — $\text{Sb}_\text{II}$ 's. The examination of the three-dimensional PATTERSON space showed that there were four peaks with definite maximum contours at levels other than zero. The comparison with the vector set map, Fig. 9, indicated these peaks as all of the second kind. In Fig. 9 these peaks are designated by letters *a*, *b*, *c*, and *d*. The computed *y* coordinate of each peak is given beside the circle indicating the location of peak. The observed *y*

Table 5. *Sb—Sb peaks used for the determination of  $y_{\text{Sb}}$ 's*

Peaks	Computed <i>y</i> 's	Observed <i>y</i> 's of the maximum contours in PATTERSON section
<i>a</i>	$y_1 + y_2$	5/60
<i>b</i>	$y_1 + y_3$ $y_2 + y_4$	10/60
<i>c</i>	$y_1 + y_4$ $y_2 + y_3$	10/60
<i>d</i>	$y_3 + y_4$	11/60

Table 6. *Determination of  $y_{\text{Sb}}$ 's from the three-dimensional PATTERSON sections, and  $\rho(xy)$  map*

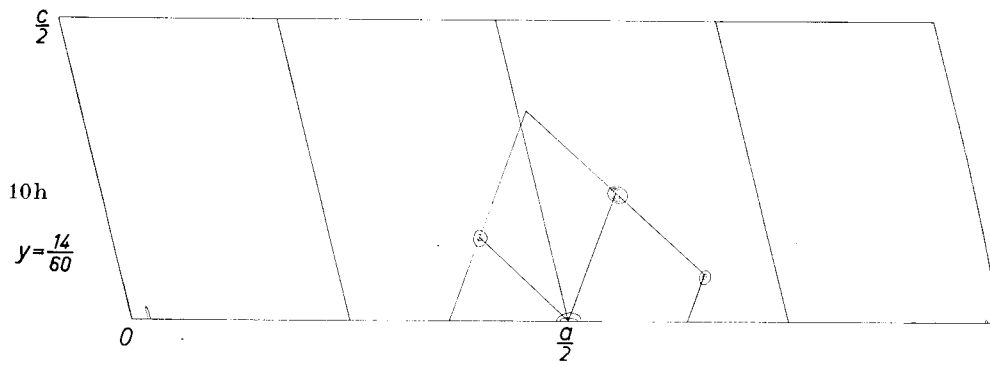
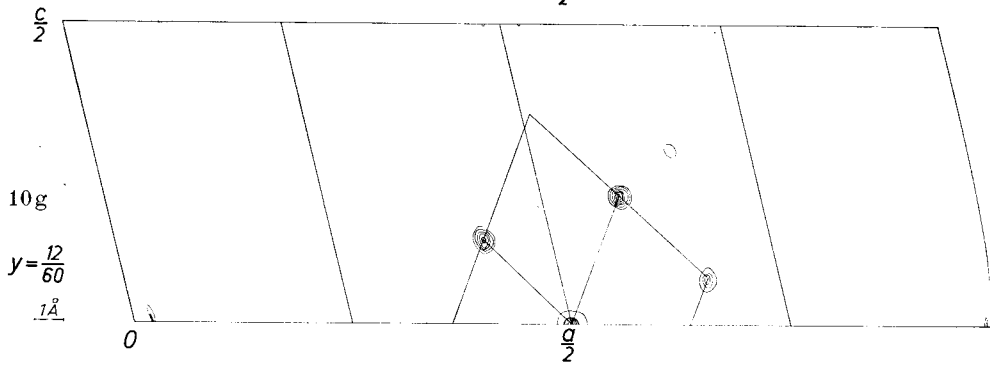
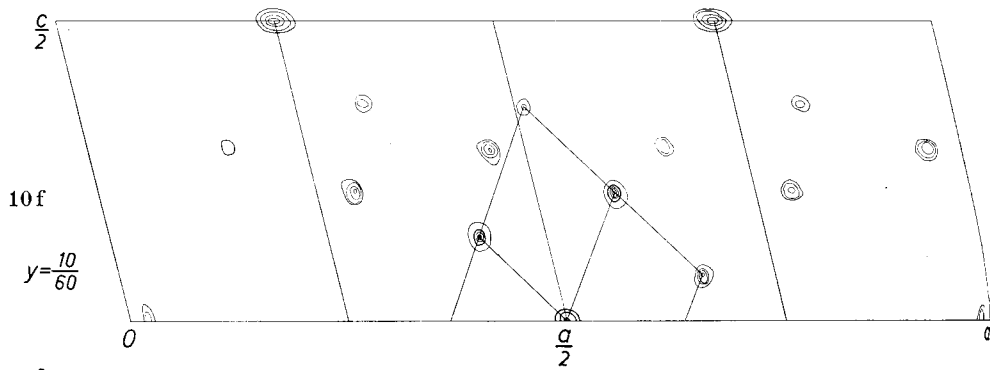
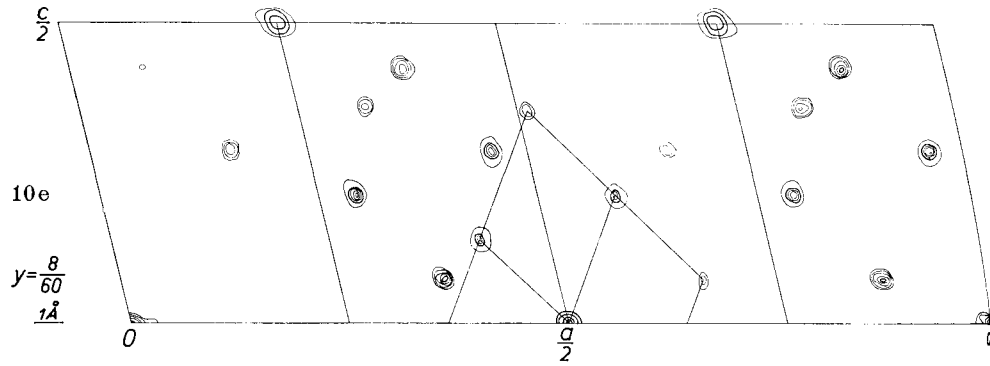
Atom	<i>y</i>		
	I From PATTERSON sections	II From $\rho(xy)$	III From least-squares refinement
$\text{Sb}_\text{I}$	$3.5/60 = 0.058$	0.056	0.063
$\text{Sb}_\text{II}$	$4.5/60 = 0.075$	0.087	0.095
$\text{Sb}_\text{III}$	$3.5/60 = 0.058$	0.056	0.064
$\text{Sb}_\text{IV}$	$4.5/60 = 0.075$	0.063	0.078

Fig. 10a. Three-dimensional PATTERSON section at  $y = 0/60$ . The heavy contours represent the fifth intervals of light contours. The details of some of the heavy peaks are omitted. All the negative contours are not shown. The maximum contours of peaks *a*, *b*, *c*, and *d* of Fig. 9 will be evident if the illustrated tetragons are traced in the following sections.

Fig. 10b. Three-dimensional PATTERSON section at  $y = 2/60$

Fig. 10c. Three-dimensional PATTERSON section at  $y = 4/60$

Fig. 10d. Three-dimensional PATTERSON section at  $y = 6/60$



coordinates of the maximum contour of these peaks are tabulated in Table 5. It is noticed that the  $y$  coordinates of these peaks have a sum form, such as  $y_1 + y_2$ . The approximate  $y$  coordinates were obtained by analyzing these values. They are tabulated in Table 6.

### Refinement of $y$ coordinates

With the approximate  $y$  coordinates of the heavy atoms determined by the above method, the structure factors  $F(hk0)$  could be computed. The resulting electron-density map  $\rho(xy)$  represents the projection of

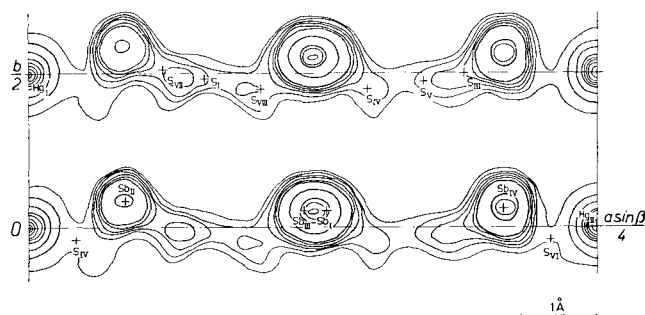


Fig. 11. Final electron-density map  $\rho(xy)$ . The asymmetric unit of projection on (001) is illustrated. Negative contours are omitted.

the structure along  $c$  axis. The refinement of the  $y$  coordinates was carried out by successive FOURIER trials with this projection. Final atomic coordinates determined in this way are tabulated in Column I of Table 7. Those of the heavy atoms are listed in Table 6. The final electron-density map  $\rho(xy)$  is shown in Fig. 11. The reliability factor for this projection was computed as  $R = 0.24$ .

### Three-dimensional refinement

The three-dimensional refinement of the structure was performed by the least-squares method developed by SAYRE<sup>14</sup> at the International

---

Fig. 10e. Three-dimensional PATTERSON section at  $y = 8/60$

Fig. 10f. Three-dimensional PATTERSON section at  $y = 10/60$

Fig. 10g. Three-dimensional PATTERSON section at  $y = 12/60$

Fig. 10h. Three-dimensional PATTERSON section at  $y = 14/60$

<sup>14</sup> P. H. FRIEDLANDER, W. LOVE and D. SAYRE, Least-squares refinement at high speed. Acta Crystallogr. 8 (1955) 732.

Table 7. *Atomic coordinates from several processes*

Atom	I	II	III
	From FOURIER maps	From first least-squares refinement	From second least-squares refinement
Hg <sub>I</sub>	$x = 0.000$	0.000	0.000
	$y = 0.500$	0.500	0.500
	$z = 0.000$	0.000	0.000
Hg <sub>II</sub>	$x = 0.250$	0.250	0.250
	$y = 0.000$	0.004	0.001
	$z = 0.000$	0.000	0.000
Sb <sub>I</sub>	$x = 0.120$	0.120	0.120
	$y = 0.056$	0.062	0.063
	$z = 0.075$	0.075	0.075
Sb <sub>II</sub>	$x = 0.042$	0.042	0.042
	$y = 0.087$	0.094	0.095
	$z = 0.213$	0.214	0.214
Sb <sub>III</sub>	$x = 0.130$	0.130	0.131
	$y = 0.056$	0.062	0.064
	$z = 0.426$	0.425	0.425
Sb <sub>IV</sub>	$x = 0.208$	0.208	0.208
	$y = 0.063$	0.073	0.078
	$z = 0.287$	0.287	0.287
S <sub>I</sub>	$x = 0.059$	0.062	0.062
	$y = 0.495$	0.503	0.493
	$z = 0.093$	0.092	0.092
S <sub>II</sub>	$x = 0.229$	0.228	0.229
	$y = 0.962$	0.026	0.028
	$z = 0.183$	0.181	0.180
S <sub>III</sub>	$x = 0.173$	0.172	0.172
	$y = 0.475$	0.510	0.506
	$z = 0.040$	0.039	0.039
S <sub>IV</sub>	$x = 0.149$	0.148	0.149
	$y = 0.450$	0.523	0.521
	$z = 0.223$	0.221	0.222
S <sub>V</sub>	$x = 0.191$	0.189	0.189
	$y = 0.488$	0.502	0.494
	$z = 0.407$	0.408	0.407
S <sub>VI</sub>	$x = 0.021$	0.022	0.022
	$y = 0.962$	0.020	0.021
	$z = 0.317$	0.318	0.318
S <sub>VII</sub>	$x = 0.077$	0.078	0.078
	$y = 0.488$	0.509	0.507
	$z = 0.460$	0.461	0.460
S <sub>VIII</sub>	$x = 0.101$	0.102	0.102
	$y = 0.450$	0.483	0.483
	$z = 0.277$	0.278	0.277

Business Machine Corp., New York. The initial atomic coordinates were these values given in Column I of Table 7. The number of structure factors used in this refinement process was 1950  $F^2(hkl)$ 's.

The reliability factor started as  $R = 0.39$ , and after three cycles of refinement went down to only  $R = 0.31$ , obviously a value too high for an acceptable structure. The atomic coordinates determined by these processes are given in Column II of Table 7.

After numerous trials, which only proved that different structure models could not improve the  $R$  factor, the result of this refinement process was closely examined. An analysis is given in Tables 8 and 9. In

Table 8. *Analysis of three-dimensional refinement cycles by the least-squares method of IBM*

	Value			
	Initial	First cycle	Second cycle	Third cycle
$K$	61.0	52.9	50.7	49.7
$B$	1.32	0.90	0.89	0.97
$R$		0.39	0.33	0.315

Table 9. *Level by level comparison of  $R$  value after second cycle*

Level	$R$ value after second cycle	$K$ optimum	$R$ value with $K_{opt}$	$K$ determined from Fig. 12	Correction factor
$k = 0$	0.354	63.6	0.172	58.1	1.00
$k = 1$	0.233	44.7	0.222	42.8	0.74
$k = 2$	0.281	38.6	0.197	39.9	0.69
$k = 3$	0.227	51.8	0.319	51.2	0.88
$k = 4$	0.664	82.1	0.489	—	

Table 8, the variations of  $R$ ,  $K$ , and averaged  $B$  values after each cycle are tabulated. In Table 9, the reliability factor computed for each level is given first. These  $R$  values are computed with a uniform scaling factor  $K$  after the second cycle, i. e., with  $K = 50.7$ . In the second column of Table 9 are given the optimum values of scaling factor  $K$ . These  $K$  values were determined by the formula,  $K = \frac{\sum F_c}{\sum F_o}$ . For example, the optimum  $K$  value of the second level is computed by the formula,  $K = \sum F_c(h2l) / \sum F_o(h2l)$ . In the third column, the  $R$  values computed with the  $K_{optimum}$  values are tabulated. The values of  $R$  given in this column are acceptable considering the

highly absorbing nature of the mineral. As a result of this analysis it was suspected that the use of a uniform scaling factor caused a large  $R$  value even if the structure was close to the final solution.

The best way to proceed was to correct the individual intensities for absorption factor. In the present case, however, as the second-best procedure, the use of a scaling factor which differed with different levels, was applied. This procedure is equivalent to the partial correction of the absorption factor.

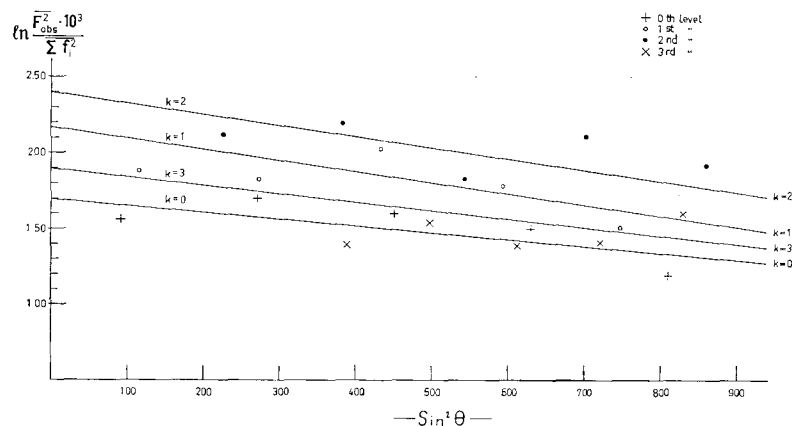


Fig. 12. Determination of non-uniform scaling factor for each level. WILSON's statistical method was applied to  $F^2(h0l)$ 's,  $F^2(h1l)$ 's,  $F^2(h2l)$ 's, and  $F^2(h3l)$ 's treated separately. The result obtained for each level is expressed by different symbols as indicated in the drawing.

These non-uniform scaling factors were determined in the following way: The observed  $F^2(hkl)$ 's with different  $K$  values were grouped together. For the  $F^2$ 's in each group, the scaling factor was determined by WILSON's<sup>12</sup> statistical method. The result of the treatment is represented in Fig. 12. The individual values of the scaling factor for each level are tabulated in the fourth column of Table 9.

Since a uniform scaling factor was necessary for the IBM procedure of refinement, the  $K$  value thus determined with the  $F^2(h0l)$ 's was used as such.  $F$  values observed for the first, second, and third levels were corrected by multiplying by the factors given in the last column of Table 9. These factors are ratios between the  $K$  value of each level to the  $K$  value of the equator.

With the  $F_o$  values thus corrected, three further cycles of refinement were carried out. The final  $R$  value was computed as 0.19. This

treatment of structure factors represents the correction of the differences between the averaged effect of absorption for different levels. The correction within each level was not considered. The final  $R$  value was considered as reasonably low. The final atomic coordinates are tabulated in Table 10, and also, for a comparison with previously obtained values, in Column III of Table 7.

The comparison between the observed and the computed structure factors is listed in Table 12.

Table 10. *Final atomic coordinates*

Atom	$x$	$y$	$z$	$B$
Hg <sub>I</sub>	0.000	0.500	0.000	1.58
Hg <sub>II</sub>	0.250	0.001	0.000	1.58
Sb <sub>I</sub>	0.120	0.063	0.075	1.09
Sb <sub>II</sub>	0.042	0.095	0.214	1.14
Sb <sub>III</sub>	0.131	0.064	0.425	0.94
Sb <sub>IV</sub>	0.208	0.078	0.287	0.21
S <sub>I</sub>	0.062	0.493	0.092	1.06
S <sub>II</sub>	0.229	0.028	0.180	0.50
S <sub>III</sub>	0.172	0.506	0.039	1.21
S <sub>IV</sub>	0.149	0.521	0.222	0.47
S <sub>V</sub>	0.189	0.494	0.407	0.96
S <sub>VI</sub>	0.022	0.021	0.318	0.76
S <sub>VII</sub>	0.078	0.507	0.460	0.85
S <sub>VIII</sub>	0.102	0.483	0.277	0.69

Note. Temperature coefficient of each atom listed under  $B$  has been determined during the refinement processes by the least-squares method.

### Discussion of the structure

The interatomic distances between the neighboring atoms are tabulated in Table 11. These distances are also shown in the diagrammatic representation of the structure, Fig. 13. In Fig. 14, the structural scheme is illustrated for the whole unit cell.

The structure of livingstonite can be described as a double-layered structure. Both kinds of layers run parallel to (001). All the Sb atoms have as closest neighbors three S atoms at distances of 2.5 Å–2.6 Å. This  $\text{SbS}_3$  unit, together with its equivalent, related by translation  $b$ , is built into a chain of composition  $\text{SbS}_2$ . There are three groups of two  $\text{SbS}_2$  chains in the structure. In one group these two  $\text{SbS}_2$  chains are related by a center of symmetry, in another by a two-fold screw axis, and in the third by no symmetry element. In all of the three cases two

